Novel technique for characterizing feature profiles in photolithography process

Fan Wang (王 帆)*, Hailiang Lu (陆海亮), Qingyun Zhang (张青云), and Anatoly Burov

Shanghai Micro Electronics Equipment Co., Ltd, Shanghai 201203, China

**Corresponding author: wangf@smee.com.cn*

Received November 15, 2011; accepted December 28, 2011; posted online March 15, 2012

A novel angle-resolved scatterometer based on pupil optimization for feature profile measurement in a photolithography process is proposed. The impact of image sensor errors is minimized by optimizing the intensity distribution of the incident light using a spatial light modulator. The scatterometry sensitivity of feature measurement at different polarization conditions is calculated using the rigorous coupled-wave and first-order analyses, and the reproducibility of the scatterometer is evaluated. The results show that the sensitivity and reproducibility of the angle-resolved scatterometer increase by 90% and 40% with pupil optimization, respectively.

OCIS codes: 120.5820, 120.3940, 050.1950.

doi: 10.3788/COL201210.061202.

As feature sizes decrease, the requirements on critical dimension (CD) uniformity have become very strict. Thus, a fast and accurate measurement technique for characterizing the CD, sidewall angle (SWA), and height of the resist profile should be established to monitor the variations in the lithography process and perform advanced process control. Various techniques such as CD-SEM[1,2], CD-AFM[3], and scatterometry[4−6] are used in profile measurement. Among these techniques, scatterometry is a highly accurate and nondeconstructive measurement technique that possesses advantages of low cost, high speed, and robustness. Angle-resolved scatterometry has already been applied to supply in-line feedback information that is necessary for tight process control[7−10].

In an angle-resolved scatterometry measurement, the profile information is extracted by modeling the angular reflection of the structure to be measured in the pupil space within a range of altitude and azimuth angles. The resist profile, including the CD, SWA, and height, is determined using the intensity distribution in the pupil image from the image sensor. In a typical angle-resolved scatterometry, the pupil intensity distribution depends on the source and optical design. The reflection at different incident angles has a large variation range and does not utilize most of the dynamic range of the image sensor.

In this letter, a novel angle-resolved scatterometer with pupil optimization is introduced. The intensity of the illumination beam is changed using a spatial light modulator, and the intensity distribution of the incident light in the pupil plane is optimized considering the feature and image sensor response properties. The first-order analysis of the scatterometry sensitivity at different polarization states is conducted on the resist-coated wafer using the rigorous coupled-wave analysis (RCWA). Based on the criterion that will be defined in the following, the sensitivities of the angle-resolved scatterometer with pupil optimization and the traditional scatterometer are compared. The reproducibility of the scatterometry on various process nodes is analyzed using the Monte Carlo method.

Figure 1 shows the schematic of the new scatterometer. The light from the source is collimated and then spatially modulated. The intensity distribution of the incident light in the pupil plane is optimized considering the feature and image sensor response properties. The collimated beam is focused onto the feature on a wafer via a projector lens, and then, the reflected light from the sample is collected using the same lens. The beam entering the receiving lens contains light reflected at different altitude and azimuth angles at different points across the sample. The light beam passes through the beam splitter, and the pupil is imaged by the relay lens. The pupil image, which represents the light reflected from the sample at different altitude and azimuth angles, is detected by the image sensor. The feature parameters, including the CD, SWA, and height, are determined using the intensity distribution in the image sensor.

The sensitivity of the scatterometry, which represents the change in the measured parameter versus a change in a sample feature, is an important characteristic and ultimately determines measurement precision. Using the first-order analysis of scatterometry sensitivity[11], the sensitivity of a traditional angle-resolved scatterometer with uniform pupil illumination can be expressed as

$$S_{\mathrm{CD}}(\theta,\,\phi) = \frac{1}{\max[R(\theta,\,\phi)]}\cdot\frac{1}{N-1}\cdot\sum_{k=1}^{N-1}\left|R_{\mathrm{CD},\,k+1}(\theta,\,\phi)-R_{\mathrm{CD},\,k}(\theta,\,\phi)\right|, \quad (1)$$

$$S_{\mathrm{SWA}}(\theta,\,\phi) = \frac{1}{\max[R(\theta,\,\phi)]}\cdot\frac{1}{N-1}\cdot\sum_{k=1}^{N-1}\left|R_{\mathrm{SWA},\,k+1}(\theta,\,\phi)-R_{\mathrm{SWA},\,k}(\theta,\,\phi)\right|, \quad (2)$$

$$S_{\mathrm{RT}}(\theta,\,\phi) = \frac{1}{\max[R(\theta,\,\phi)]}\cdot\frac{1}{N-1}\cdot\sum_{k=1}^{N-1}\left|R_{\mathrm{RT},\,k+1}(\theta,\,\phi)-R_{\mathrm{RT},\,k}(\theta,\,\phi)\right|, \quad (3)$$

 © 2012 Chinese Optics Letters

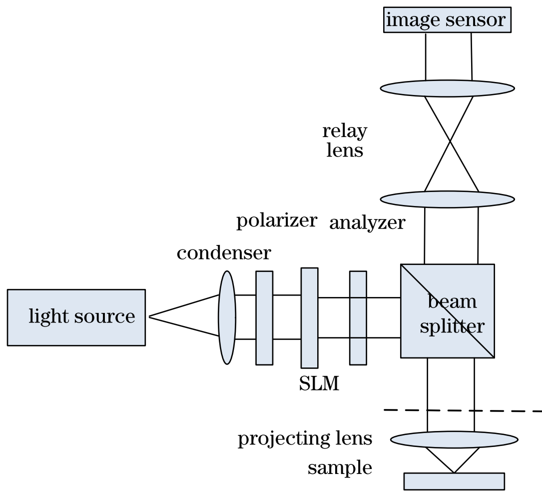

Fig. 1. Schematic diagram of the angle-resolved scatterometer with pupil optimization.

where θ and ϕ represent the altitude and azimuth angles, respectively, R represents the reflectivity of the specified feature at a specified angle, k represents an index given to each test site with varying profiles, and N denotes the number of test sites containing geometric parameters. The subscripts CD, SWA, and RT represent critical dimension, sidewall angle, and resist height, respectively. An average is appropriate if the increment is small and if the changes are comparable in magnitude from the reflectivity to the next. From Eqs. (1)–(3), the sensitivity of the specified altitude and azimuth angles is influenced by the reflectivity response to variations in geometric parameters and the maximum reflectivity in the pupil space.

The sensitivity of the specified altitude and azimuth angles can be optimized via pupil optimization. The detector response with uniform pupil illumination is calculated using the RCWA and sensor-response models. The intensity of the illumination beam is changed by a spatial light modulator to induce a similar response in the pixels in the image sensor. The sensitivity of the angle-resolved scatterometer with pupil optimization as a function of the specified altitude and azimuth angles can be expressed as

$$S'_{\mathrm{CD}}(\theta,\phi)=\frac{1}{R(\theta,\phi)}\cdot\frac{1}{N-1}\cdot\sum_{k=1}^{N-1}|R_{\mathrm{CD},\,k+1}(\theta,\phi)-R_{\mathrm{CD},\,k}(\theta,\phi)|, \quad (4)$$

$$S'_{\mathrm{SWA}}(\theta,\phi)=\frac{1}{R(\theta,\phi)}\cdot\frac{1}{N-1}\cdot\sum_{k=1}^{N-1}|R_{\mathrm{SWA},\,k+1}(\theta,\phi)-R_{\mathrm{SWA},\,k}(\theta,\phi)|, \quad (5)$$

$$S'_{RT}(\theta,\phi)=\frac{1}{R(\theta,\phi)}\cdot\frac{1}{N-1}\cdot\sum_{k=1}^{N-1}|R_{\mathrm{RT},\,k+1}(\theta,\phi)-R_{\mathrm{RT},\,k}(\theta,\phi)|. \quad (6)$$

From Eqs. (4)–(6), the sensitivity of the low reflectivity angle is improved using pupil optimization.

The sensitivity of the geometric parameters was calculated as a function of the altitude and azimuth angles for the traditional and pupil-optimized scatterometers by employing the RCWA[12,13]. The measurement wavelength of the scatterometer is assumed to be 632.8 nm with p- and s-polarized illuminations, and a 0.93-NA microscope lens is used. As illustrated in Fig. 2, the sample consists of a resist layer, a bottom antireflective coating (BARC) layer, and a silicon substrate. The thickness of the BARC layer is 30 nm. The nominal RT, SWA, and CD are 72 nm, 85°, and 32 nm, respectively. The steps from each test site to the next correspond to nominal CD, SWA, and RT increments of 0.23 nm, 0.31°, and 0.082 nm, respectively.

The sensitivity results simulated with p-polarized light are shown in Fig. 3. Figures 3(a) and (d), (b) and (e), and (c) and (f) display the sensitivity contours of

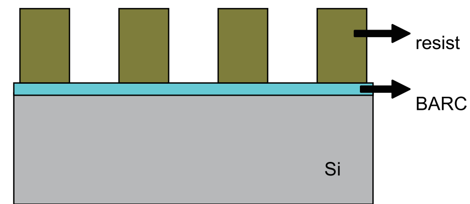

Fig. 2. Cross section of the sample.

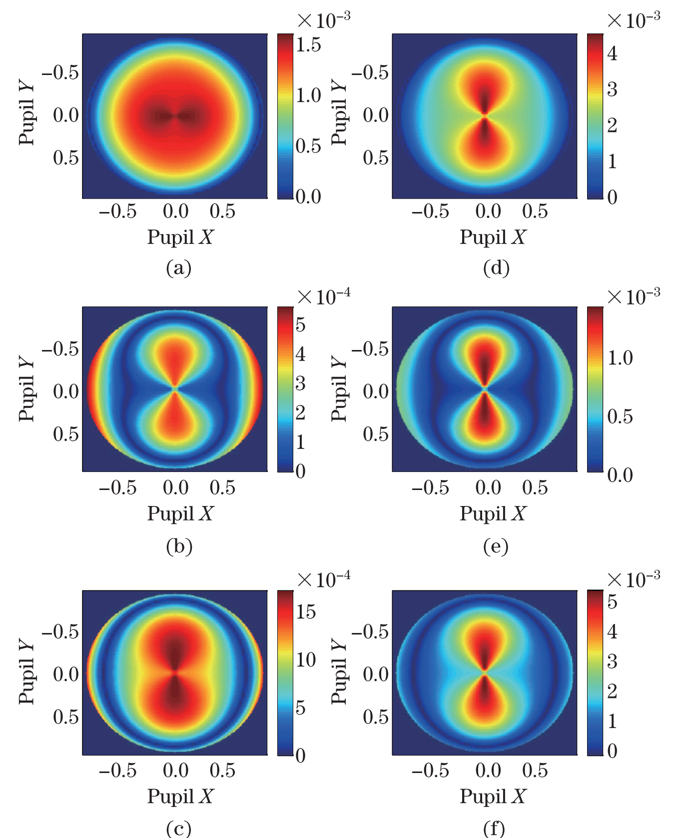

Fig. 3. Sensitivity contours of the p-polarized light in the pupil plane. (a) CD, (b) SWA, and (c) RT sensitivities in the traditional scatterometer. (d) CD, (e) SWA, and (f) RT sensitivities in the scatterometer with pupil optimization.

the CD, SWA, and RT, respectively, for the traditional and pupil-optimized scatterometers. From Fig. 3, the maximum RT and SWA sensitivities of the p-polarized light in the tradition scatterometer are on the edge of the pupil, suggesting that the light with a large altitude angle has to be detected using a high NA microscope to ensure profile measurement accuracy. The maximum sensitivity of the p-polarized light for the pupil-optimized scatterometer is closer to the center of the pupil, indicating that the projection lens could have a smaller NA. The average sensitivities over the pupil space are shown in Table 1. According to Table 1, the average sensitivities of the CD, SWA, and RT increase by 101%, 91%, and 95%, respectively, with pupil optimization.

Similar sensitivity results with s-polarized light are shown in Fig. 4. From Fig. 4, the maximum sensitivity of the s-polarized light in the traditional scatterometer is also on the edge of the pupil, whereas the maximum sensitivity of the p-polarized light for the pupil-optimized scatterometer is closer to the center of the pupil. The NA of the projecting lens could be reduced via pupil optimization. The average sensitivities over the pupil space are shown in Table 1. According to Table 1, the average sensitivities of the CD, SWA, and RT increase by 171%, 151%, and 168%, respectively, with pupil optimization.

The Monte Carlo method was employed to analyze the impact of the image sensor noise on the measurement result of the geometric parameters. White Gaussian noise was generated on the theoretical image calculated using the specified geometric parameters. Using images with sensor noise, the CD, SWA, and RT were extracted. The reproducibilities of the CD, SWA, and RT for the traditional and pupil-optimized scatterometers with 0.1% image noise are shown in Fig. 5. The results show that the reproducibilities improve by 44%, 50%, and 45%, respectively, with pupil optimization.

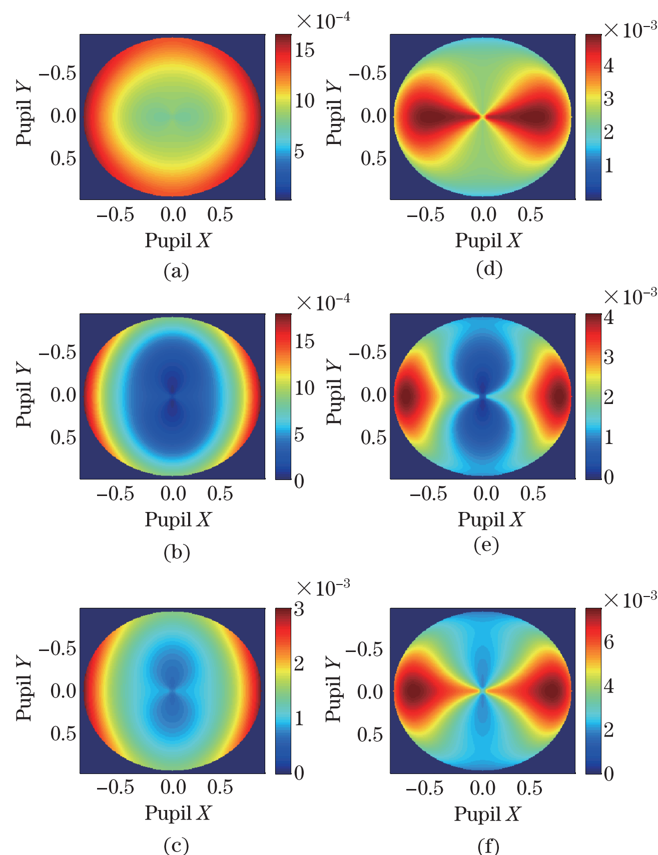

Fig. 4. Sensitivity contours of the s-polarized light in the pupil plane. (a) CD, (b) SWA, and (c) RT sensitivities in the traditional scatterometer. (d) CD, (e) SWA, and (f) RT sensitivities in the scatterometer with pupil optimization.

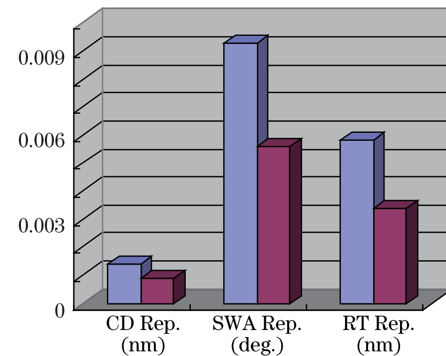

Fig. 5. (Color online) Reproducibility of the geometric parameters for the traditional (blue) and pupil-optimized (purple) scatterometers.

Table 1. Average Sensitivities of the CD, SWA, and RT under Different Conditions

Type	Polarization	CD ($\times10^{-4}$)	SWA ($\times10^{-4}$)	RT ($\times10^{-4}$)
Traditional	p-polarized	8.79	2.31	9.00
Pupil Optimized	p-polarized	17.60	4.40	17.50
Traditional	s-polarized	11.48	7.45	15.20
Pupil Optimized	s-polarized	31.10	18.70	40.80

In conclusion, a novel angle-resolved scatterometer based on pupil optimization is proposed for feature profile measurement. Pupil optimization can improve the measurement accuracy of the angle-resolved scatterometer. According to the simulation results, the sensitivity and reproducibility of the geometric parameters of the profile measurements increase by more than 90% and 40%, respectively, with pupil optimization.

References

1. C. Archie, E. Solecky, P. Rawat, T, Brunner, K. Yoshimoto, R. Cornell, and O. Adan, Proc. SPIE **7638,** 763804 (2011).
2. K. Takamasu, H. Okitou, S. Takahashi, M. Konno, O. Inoue, and H. Kawada, Proc. SPIE **7971,** 797108 (2011).
3. J. Foucher, N. Rana, and C. Dezauzier, Proc. SPIE **7638,** 763802 (2010).
4. B. Bilski, K. Frenner, and W. Osten, Opt. Express **19,** 19967 (2011).
5. I. Gereige, S. Robert, S. Thiria, F. Badran, G. Granet, and J. J. Rousseau, J. Opt. Soc. Am. A **25,** 1661 (2008).
6. C. Tan, Y. Chan, J. Chen, T. Liao, and M. Chiu, Chin. Opt. Lett. **9,** 101202 (2011).
7. C. Ko and Y. Ku, Opt. Express **14,** 6001 (2006).
8. Y. Cohen, J. Finders, R. Knops, O. Mouraille, I. Minnaert-Janssen, F. Duray, E. Mos, A. Kremer, A.

Sagiv, S. Mangan, M. B. Yishay, H. Dai, C. Bencher, C. Ngai, K. Dotan, and I. Englard, Proc. SPIE **7971,** 79711N (2011).

9. R. M. Silver, B. M. Barnes, R. Attota, J. Jun, M. Stocker, E. Marx, and H. J. Patrick, Appl. Opt. **46,** 4248 (2007).
10. T. Novikova, A. Martino, S. Hatit, and B. Drévillon, Appl. Opt. **45,** 3688 (2006).
11. T. Miyakawa, K. Sentoku, K. Sato, and H. Ina, Proc. SPIE **7637,** 763721 (2010),.
12. M. G. Moharam and T. K. Gaylord, J. Opt. Soc. Am. **71,** 811 (1981).
13. M. G. Moharam, E. B. Grann, D. A. Pomment, and T. Gaylord, J. Opt. Soc. Am. A **12,** 1068 (1995).